Petroleum Science 20 (2023) 102–113

Contents lists available at ScienceDirect

Petroleum Science

journal homepage: www.keaipublishing.com/en/journals/petroleum-science

Original Paper

Quantitatively unmixing method for complex mixed oil based on its fractions carbon isotopes: A case from the Tarim Basin, NW China

Tao-Hua He [a, b, e], Wen-Hao Li [b, e, *], Shuang-Fang Lu [c, e, **], Er-Qiang Yang [b], Tao-Tao Jing [e], Jun-Feng Ying [b], Peng-Fei Zhu [b, e], Xiu-Zhe Wang [b], Wen-Qing Pan [d], Bao-Shou Zhang [d], Zhong-Hong Chen [b]

[a] Key Laboratory of Oil and Gas Resources and Exploration Technology, Yangtze University, Wuhan, Hubei 430100, China
[b] School of Geosciences, China University of Petroleum (East China), Qingdao, Shandong, 266580, China
[c] Sanya Offshore Oil & Gas Research Institute, Northeast Petroleum University, Sanya, Hainan 572025, China
[d] Petroleum Exploration & Production Research Institute, Tarim Oilfield Company, PetroChina, Korla, Xinjiang, 841000, China
[e] Key Laboratory of Deep Oil and Gas, China University of Petroleum (East China), Qingdao, Shandong, 266580, China

ARTICLE INFO

Article history:
Received 26 October 2021
Received in revised form
26 February 2022
Accepted 28 July 2022
Available online 5 August 2022

Edited by Jie Hao and Teng Zhu

Keywords:
Mixed crude oil
Carbon isotopes
End-member oil
De-convolution
Secondary alteration
Tarim Basin

ABSTRACT

Deep mixed oils with secondary alterations have been widely discovered in the Tarim Basin, but current methods based on biomarkers and isotopes to de-convolute mixed oil cannot calculate the exact mixing proportion of different end-member oils, which has seriously hindered further exploration of deep hydrocarbons in the study area. To solve this problem, we constructed a novel method based on the carbon isotope ($\delta^{13}C$) of the group components to de-convolute mixed liquid hydrocarbons under the material balance principle. The results showed that the mixed oil in the Tazhong Uplift was dominantly contributed at an average proportion of 68% by an oil end-member with heavier $\delta^{13}C$ that was believed to be generated from the Cambrian-Lower Ordovician source rocks, whereas the mixed oil in the Tabei Uplift was predominantly contributed at an average proportion of 61% by an oil end-member with lighter $\delta^{13}C$ that was believed to be generated from the Middle-Upper Ordovician source rocks. This indicates that, on the basis of the detailed description of the distribution of effective source rocks, the proposed method will be helpful in realizing differential exploration and further improving the efficiency of deep liquid hydrocarbon exploration in the Tarim Basin. In addition, compared to traditional $\delta^{13}C$ methods for whole oil and individual n-alkanes in de-convoluted mixed oil, the proposed method has a wider range of applications, including for mixed oils with variations in color and density, indicating potential for promoting the exploration of deep complex mixed oils in the Tarim Basin and even around the world.

1. Introduction

With the increasingly prominent contradiction between the supply and demand of petroleum resources and the increasing exploration and development of conventional medium-shallow hydrocarbons in China (Huang et al., 2016; Li et al., 2022; Sun et al., 2022), finding new petroleum resources is becoming increasingly difficult (Chen et al., 2019; Zhu et al., 2019a, 2020; Cheng et al., 2020; Li et al., 2020; Hu et al., 2021a, b). Fortunately, the deepened lower limit of the liquid hydrocarbon production layer (the depth of the production layer of the Luntan 1 well in the Tarim Basin is > 8200 m) suggests that deep and ultra-deep hydrocarbon exploration has become a trend in oil and gas exploration, also providing an important and realistic resource worldwide (Zhu et al., 2012; Zhang et al., 2015; Huang et al., 2016; Li et al., 2017; He et al., 2020a; Yang et al., 2020). However, complex mixed oil is one of the most typical oils encountered during deep oil exploration field, being a hot and challenging aspect in the field of oil and gas geochemistry (He et al., 2022a, 2022b). Deep complex mixed oil is mainly produced by the mixing of oil from (1) different source rocks, (2) homologous source rocks from different periods, (3) different

* Corresponding author. School of Geosciences, China University of Petroleum, Qingdao, Shandong, 266580, China.
** Corresponding author. Key Laboratory of Deep Oil and Gas, China University of Petroleum (East China), Qingdao, Shandong, 266580, China.
E-mail addresses: liwh@upc.edu.cn (W.-H. Li), lushuangfang@upc.edu.cn (S.-F. Lu).

https://doi.org/10.1016/j.petsci.2022.07.010

source rocks in different periods, and (4) homologous/non-homologous source rocks after different degrees of secondary alteration (biodegradation, thermal sulfate reduction, thermal alteration, and/or gas washing) (Zhang et al., 2004a, b, 2015; Cai et al., 2015; Huang et al., 2016, 2017; Zhan et al., 2016; Zhu et al., 2018, 2019b, 2020). To qualitatively reveal the relative contributions of different source rocks, five methods were proposed: (1) artificial mixing of end-member oil to establish a plate for qualitatively de-convoluting mixed oil (Arouri and McKirdy, 2005); (2) determining carbon isotopic ($\delta^{13}C$) compositions, including the $\delta^{13}C$ compositions of whole oil and the compound-specific $\delta^{13}C$ compositions of n-alkanes (Li et al., 2015; Pang et al., 2016); (3) mathematical calculations based on the concentrations of selected biomarkers and whole oil carbon isotopic ($\delta^{13}C_{oil}$) compositions (Chen et al., 2003, 2007); (4) using source- or age-specific biomarkers (Dzou et al., 1999); and (5) alternating least squares analysis using biomarker concentration data or related biomarker parameters (such as ratios and $\delta^{13}C$) (Peters et al., 2008; Zhan et al., 2016). The effectiveness of the above methods mainly depends on undamaged biomarkers, $\delta^{13}C$, as well as the choice of end-member oil (EMO) (Huang et al., 2016). The quantitative methods proposed above are mainly applicable to the binary or ternary mixing of shallow conventional hydrocarbons, however, they cannot be applied to de-convolute the deep complex mixed oils. Deep hydrocarbon accumulation is complex, and characterized by large deep burials, multi-stage accumulations, multi-stage adjustments and multi-stage secondary alterations in the superimposed basin, resulting in the limited effectiveness of steroid, terpene, aromatic biomarker parameters (concentration and ratio) (Zhang et al., 2004a; Peters et al., 2005). In addition, the $\delta^{13}C$ of selected n-alkanes can only represent the isotopic composition of saturated hydrocarbons (SAs), but not that of the entire mixed oil. Similarly, the carbon isotope of mixed oil ($\delta^{13}C_m$) leads to multiple solutions. For example, thermally altered mixed oil with a high content of SAs and low asphaltene (AS) content and biodegradable mixed oil with a low content of SAs and a high AS content may have the same carbon isotope, but this does not mean that their mixed processes are the same in the Tarim Basin. In addition, deep and ultra-deep oils have undergone varying degrees of secondary alterations, suggesting that effective EMOs cannot be found (Huang et al., 2016). These difficulties have posed serious challenges to estimating the relative contributions of different source rocks, considerably hindering the pace of deep-to-ultra-deep petroleum exploration.

The $\delta^{13}C$ of the free liquid hydrocarbon group components (GRCs) changes little during reservoir formation (Liu et al. 2008). If we assume that all mixed oils are first mixed by different GRCs and later mixed again, then establishing a comprehensive de-convoluting mixed oil method based on group component carbon isotopes ($\delta^{13}C_{GRC}$) can quantitatively reveal the relative contributions of different GRCs. Finally, the mixing proportion can be calculated on the basis of the weighted average of the relative GRC contents from different EMOs. Thus, taking the Lower Paleozoic mixed oil from the Tarim Basin as an example, our purpose in this study was to establish a new de-convoluting mixed oil method and calculate the relative contribution from each EMO, which can promote the exploration of complex mixed oil in the Tarim Basin.

2. Geological setting

The Tarim Basin is located between the Kunlun and Tianshan Mountains, bounded by the Altun Mountain Fault Zone in the east, covering a total area of 56×10^4 km^2. The basin is a large craton with a large buried depth of Paleozoic marine assemblage, mainly 6000–12000 m (Zhang et al., 2004a). Affected by its complex tectonic background, the Tarim Basin has experienced many thermal events and multistage tectonic evolution throughout geological history (Huang et al., 2016). Generally, Mesozoic and Cenozoic continental foreland basins are superimposed on the Sinian-Paleozoic marine craton basins. Currently, four uplift and five depression structures can be found in this basin. The four uplift structures are Tabei, Tazhong, Tadong and Bachu Uplifts, respectively; five depression structures are the Kuche, Northern, Southwest, Tanggu and Southeast Depressions, respectively (Fig. 1) (Pan et al., 2015).

Three large-scale extensional and three large-scale compressional activities have developed over the geological historical period, forming three structural belts and six large unconformities, which provided migration channels for hydrocarbons generated in the Lower Paleozoic and created reservoir space (relatively developed cracks, dissolution pores, fault-dissolved bodies) (Zhang et al.,

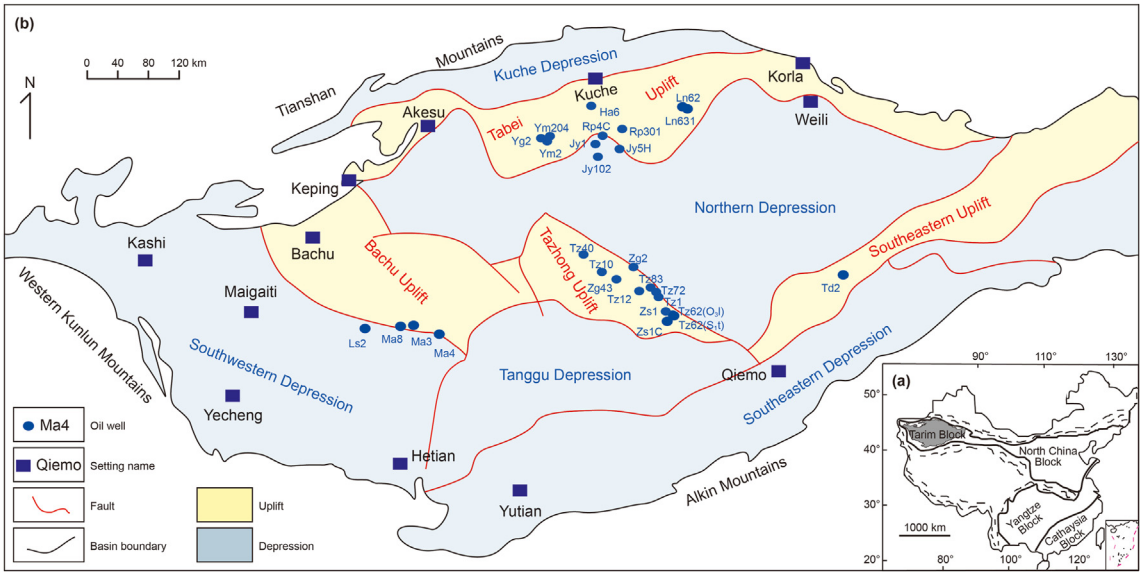

Fig. 1. (a) A simplified tectonic map of China showing the location of the Tarim Block. The inset gray area shows the location of Fig. 1b. (b) The location of typical oil wells sampled in the Tarim Basin (Pan et al., 2015).

Table 1
Information of typical marine oil samples in the Tarim Basin.

SN.	Well number	Top depth, m	Bottom depth, m	Strata	Structural location	Oil type*
WO01	Ln631	5800.81	5845.00	O_2y	Tabei Area	I
WO02	Ma4	1800.34	2041.20	$C_1b + O_2y$	STBA	I
WO03	Xk7C	6900.00	6930.00	Oy	Tabei Area	II
WO04	Tz83	5433.00	5441.00	O_3l	Tazhong Area	II
WO05	Ym204	5845.00	5920.50	O_2y	Tabei Area	II
WO06	Tz40	4306.00	4340.00	Cd	Tazhong Area	II
WO07	Ma3	1508.00	1518.00	O_3l	STBA	I
WO08	Ha6	5953.00	5954.00	C	Tabei Area	II
WO09	Tz62	4700.50	4758.00	O_3l	Tazhong Area	II
WO10	Ym102	7249.03	7313.00	O_3l	Tabei Area	II
WO11	RP4C	6918.42	7026.12	O_3l	Tabei Area	II
WO12	JY5H	7043.00	7255.00	$O_{2\text{-}3}y$	Tabei Area	II
WO13	Zg2	5866.00	5893.00	O_3l	Tazhong Area	II
WO14	Rp301	7006.00	7069.00	O_2y	Tabei Area	II
WO15	Ma3	1414.00	1424.00	Cb	STBA	I
WO16	Ls2	5741.00	5830.00	O_1p	STBA	I
WO17	Tz72	5428.00	5561.73	O_3l	Tazhong Area	II
WO18	Zs1C	6861.00	6944.00	ϵ_1x	Tazhong Area	I
WO19	Qun6	5507.69	5588.69	D_3d	STBA	I
WO20	Tz10	4616.32	5350.00	S_1t- S_1k	Tazhong Area	II
WO21	Tz62	4052.88	4075.58	S_1t	Tazhong Area	II
WO22	Tz12	4339.50	4413.50	S_1k	Tazhong Area	II
WO23	Zg43	4800.00	5334.09	O_1y	Tazhong Area	II
WO24	Ma4	2018.00	2022.00	O_2y	STBA	I
WO25	Tz103	3743.00	3746.00	D_3d	Tazhong Area	II
WO26	Ma8	1488.56	1569.21	C_1b	STBA	I
WO27	Tz1	3659.00	3684.00	ϵ	Tazhong Area	II
WO28	Ym2	3597.68	6050.00	Oy	Tabei Area	II
WO29	Yg2	6041.00	6125.00	O	Tabei Area	II
WO30	Tz10	4206.00	4230.00	Cd	Tazhong Area	II
WO31	Rp3	6977.20	7040.00	O_2y	Tabei Area	II
WO32	Zs1	6426.00	6497.00	ϵ_2a	Tazhong Area	II
WO33	Jy1	7154.61	7208.40	O_2y	Tabei Area	II
WO34	Tz1	3659.00	3684.00	O	Tazhong Area	II
WO35	Ln62	5565.00	5578.00	D_3d	Tabei Area	I

Note: SN., the oil sample number; *Oil type identified by the Suppl. Figs. S1–S5; STBA, southwestern Tarim Basin area.

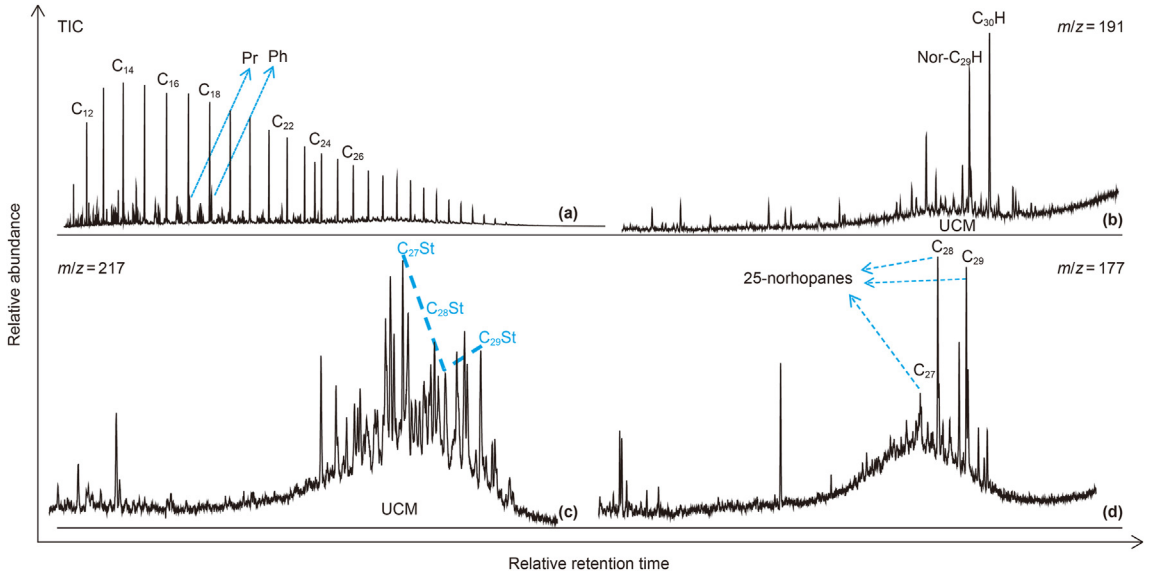

Fig. 2. Partial mass chromatograms of TIC, *m/z* 191, 217, and 177 for the saturated fraction of sample WO04 (UCM, unrecognized complex materials; H, hopane; St, sterane).

2004a). Among these activities, during the collision orogeny at the end of Caledonian and Early Hercynian, large-scale crustal uplifts developed in the Tabei, Tazhong and Bachu Uplifts, resulting in the denudation and biodegradation of early filled reservoirs, which led to a set of asphalt sandstones with an area of 2.53×10^4 km^2 and a maximum thickness of up to 152.5 m (Well Ha1). This set of asphalt sandstones represents a large-scale hydrocarbon accumulation and destruction, and the results of calculating ancient reservoir restoration showed that the corresponding hydrocarbon resource destruction has been more than 133×10^8t (Zhang et al., 2004b, 2011; Tian et al., 2008; He et al., 2020a).

Compared with the Ordos and Sichuan Basins (both cratonic basins), which are rich in gas, the above distinctive tectonic activities promoted a complex hydrocarbon accumulation process

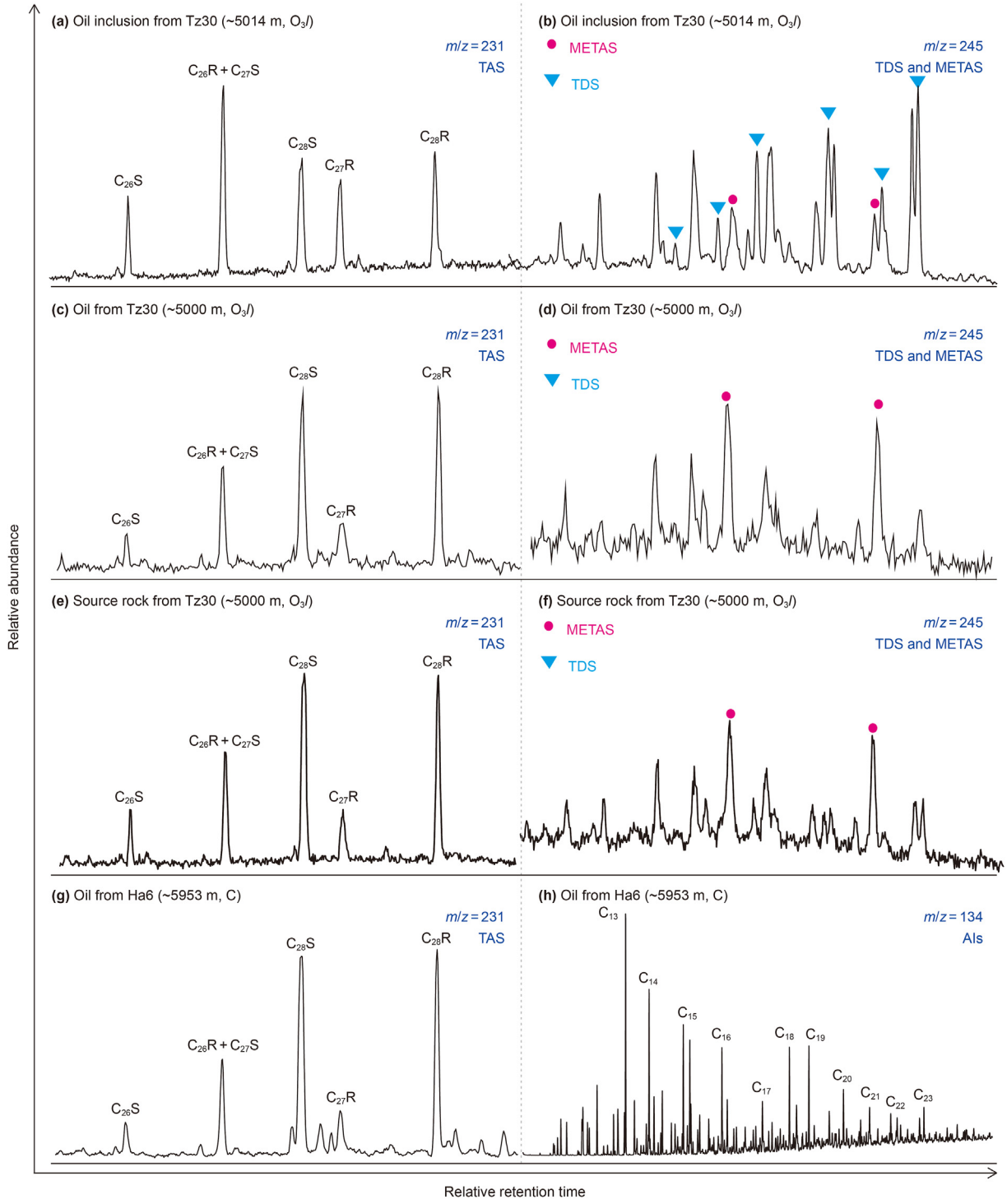

Fig. 3. Representative mass chromatograms of *m/z* 231, 245, and 134 for oil, oil inclusion and source rock samples (TAS, triaromatic sterane; TDS, triaromatic dinosteranes; METAS, 3-methyl-24-ethyl-triaromatic sterane; AIs, aryl isoprenoids).

involving multi-stage accumulation and multi-stage secondary transformation/redistribution, which is also one of the fundamental reasons for abundant liquid hydrocarbon resources developed in the Tarim Basin. These resources are thought to be derived from Cambrian-Lower Ordovician and Middle-Upper Ordovician strata, but which one has been the main contributor of known oil fields remains controversial (Sun et al., 2003; Cai et al., 2009; Li et al., 2012; Huang et al., 2016; Xiao et al., 2016; He et al., 2022b).

3. Sample and methods

We collected a total of 35 typical marine oil samples from the Tarim Basin, including 15 samples from 12 wells in the Tazhong area, 13 samples from 13 wells in the Tabei area, and 7 samples from 5 wells in the Bachu area (Table 1). The strata of the above oil samples included Cambrian, Ordovician, Silurian, Devonian and Carboniferous strata, from old to new. The burial depth of the oil

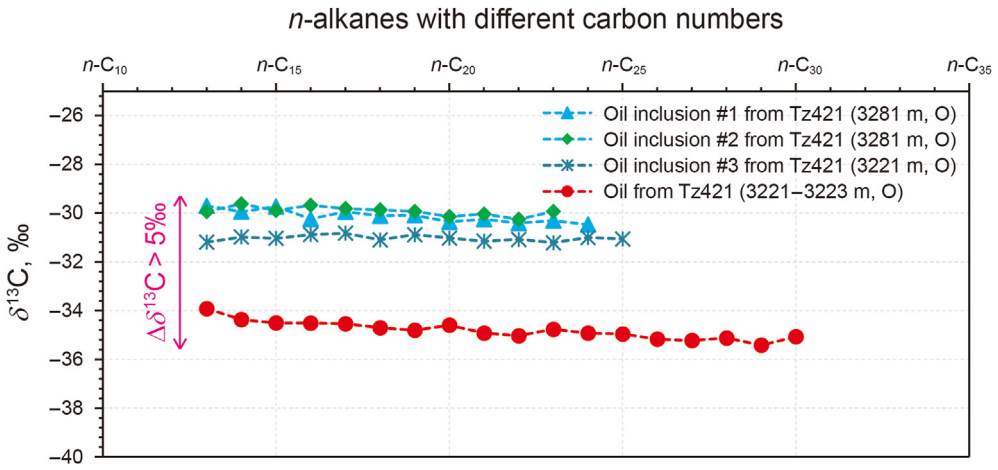

Fig. 4. Compound-specific $\delta^{13}C$ of n-alkanes for oil and oil inclusion of Well Tz421.

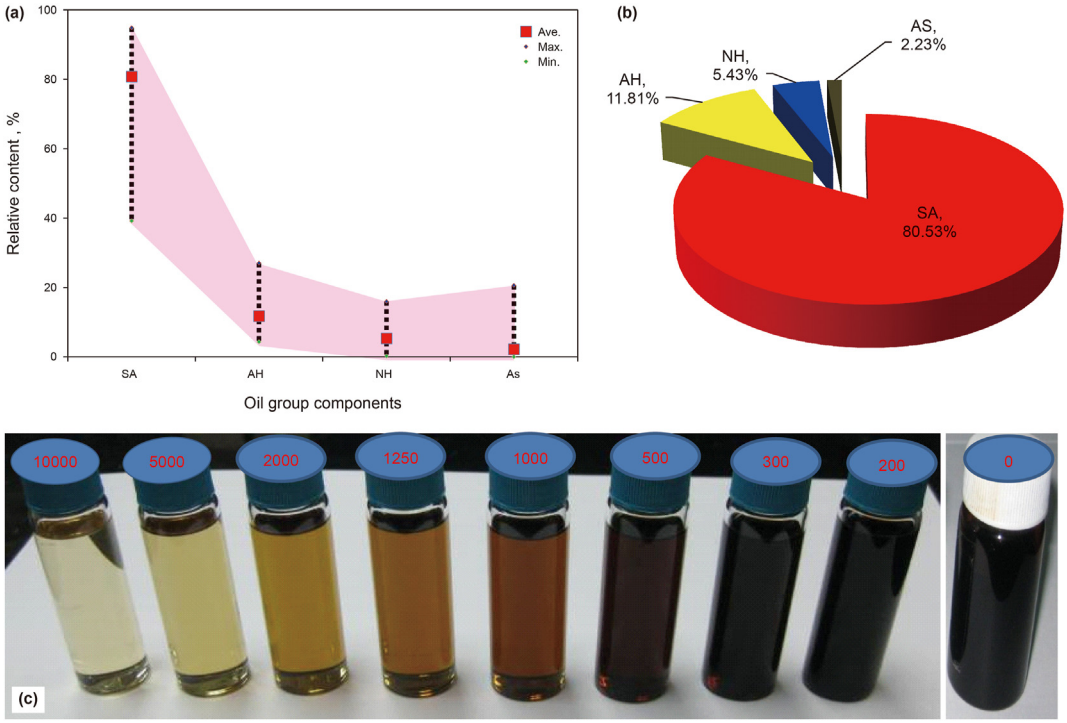

Fig. 5. Relative and average content distribution of group components (a, b, respectively) and dilution model of mixed source oil (c) (Note: max, maximum; min, minimum; ave, average; SA, saturated hydrocarbon; AH, aromatic hydrocarbon; NH, non-hydrocarbon; AS, asphaltene; number on bottle cap indicates dilution times of heavy oil by dichloromethane in the simulation experiment).

reservoirs sampled above ranged from 1414 to 7249 m. Deep oil samples (buried depth >4500 m) accounted for 66%, and ultra-deep oil samples (buried depth >6000 m) accounted for 29%. The properties of crude oil ranged from light condensate (such as Well Zs1C, 6861.00–6944.00 m) to heavy biodegradable oil (such as Well Rp4C, 6918.42–7026.12 m), in which light oil accounted for about 69% and heavy oil accounted for about 31% of the total. Therefore, the selected oil samples represented reservoirs with different structural zones, buried depths and properties in the Tarim Basin.

We separated all the oil samples into SAs, aromatic hydrocarbon (AH), non-hydrocarbon (NH) and AS using liquid column chromatography. We tested the $\delta^{13}C$ of oil and the above four fractions on an EA-MAT 253 PLUS joint instrument at the Key Laboratory of Deep Oil and Gas from China University of Petroleum (East China). We tested each sample at least three times, with a test error of less than 0.3‰. The SAs were analyzed using a SHIMADZU GC-2010Plus equipped with an FID. We analyzed SAs and AH by gas chromatography-mass spectrometry (GC-MS) on a SHIMADZU GC-2010/GC-2010Plus-MS OP2010 Ultra. Further details are provided in our previous works (He et al., 2018, 2019, 2020a, b). We further treated SAs with urea adduction to separate n-alkanes, iso-alkanes, and cyclic-alkanes. We analyzed the compound-specific $\delta^{13}C$ of n-alkanes from each SA by gas chromatography–isotope ratio mass spectrometry (GC-IRMS) on a GV Isoprime IRMS instrument interfaced with an HP6890 gas chromatograph via a combustion interface. We tested each sample at least twice, and the reproducibility was generally within ±0.4‰ (Yu et al., 2012).

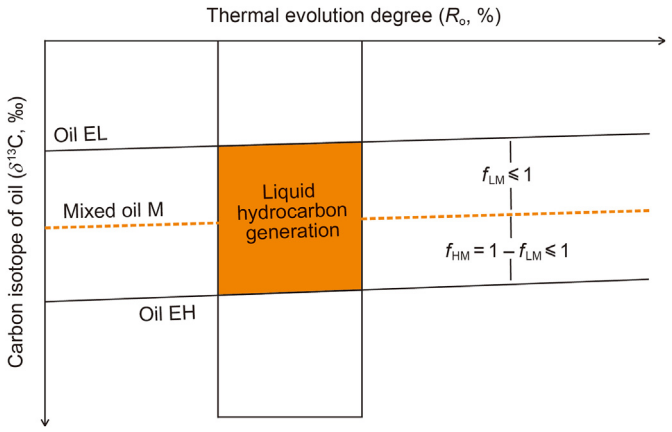

Fig. 6. $\delta^{13}C$ characteristics of two end-member oils and mixed oil (Pang et al., 2016) (LE, end-member oil with lighter $\delta^{13}C$; HE, end-member oil with heavier $\delta^{13}C$; f_{LM}, the contribution from LE to mixed oil M; f_{HM}, the contribution from HE to mixed oil M).

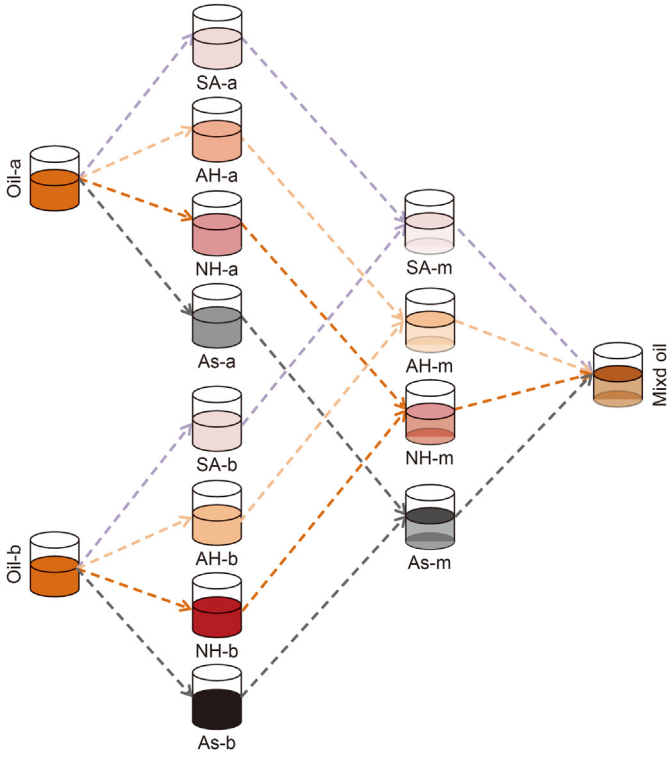

Fig. 7. Conceptual model of mixed oil (Note: SA, saturated hydrocarbon; AH, aromatic hydrocarbon; NH, non-hydrocarbon; AS, asphaltene; m, mixed).

4. Extremely common mixed-oil phenomenon

4.1. Mixing of biodegraded and non-biodegraded oils

Biodegraded oil is created through an alteration of the oil produced by living organisms. The most typical difference between biodegraded and non-biodegraded oils is whether there is a complete distribution of n-alkanes or unresolved complex mixture (UCM) or whether there are biodegraded products (such as 25-norhopanes and seco-hopanes) (Peters et al., 2005). The test results showed that most of the black heavy oils in the study area contain biodegraded oil. Most typically, the complete distribution

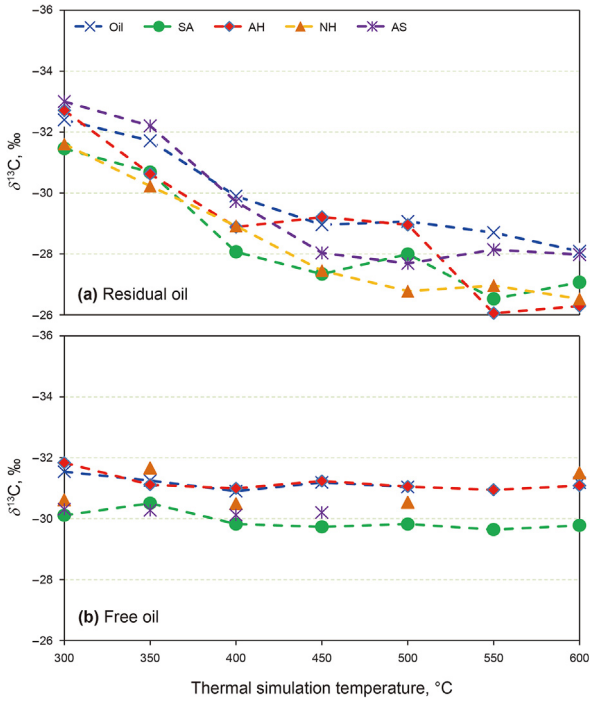

Fig. 8. $\delta^{13}C$ characteristics of residual/free oil and their group components under thermal simulation experiments (Note: SA, saturated hydrocarbon; AH, aromatic hydrocarbon; NH, non-hydrocarbon; AS, asphaltene) (Liu, 2008).

of n-alkanes showed that the WO04 oil sample may not undergo obvious biodegradation (Fig. 2a); however, the WO04 oil sample also contained obvious UCM and abundant 25-norhopane (C_{27}, C_{28} and C_{29}) (Fig. 2b–d), indicating that this oil had undergone obvious biodegradation. The most reasonable explanation is that the oil accumulated in the early stage was biodegraded during tectonic uplift, whereas the oil accumulated in the late stage was not biodegraded after tectonic subsidence to the lower limit of anaerobic microbial survival. Therefore, the WO04 oil sample was a mixture of biodegraded and non-biodegraded oils.

4.2. Mixing of early- and late-generated oils

Theoretically, the difference between early- and late-generated oils can be reflected in maturity and biomarker indicators (Peters et al., 2005). However, deep liquid hydrocarbons are usually the products of source rocks that experienced high thermal evolution, and their maturity differences are relatively less apparent because the relevant maturity indicators (isomerization parameters) might reach an endpoint (or equilibrium value) and cannot effectively indicate maturity. The correlation of biomarkers and isotopes between oil and oil inclusions from the same trap is an appropriate choice for differentiation of oil maturity because the information recorded from the early-generated oil trapped in the reservoir. This correlation of stable biomarkers in the Tazhong Uplift suggests that differences exist in triaromatic sterane (TAS), triaromatic dinosteranes (TDS), 3-methyl-24-ethyl- triaromatic sterane (METAS), and aryl isoprenoids (Fig. 3a–f). Taking Well Tz30 as an example, we found a strong correlation between the source rock (~5000 m) and oil sample (~5000 m) in terms of abundant C_{28} TAS and METAS levels but low TDS levels (Fig. 3c–f), indicating that the oil came from this type of source rock; however, we noted differences between oil and oil inclusions at similar locations because of the

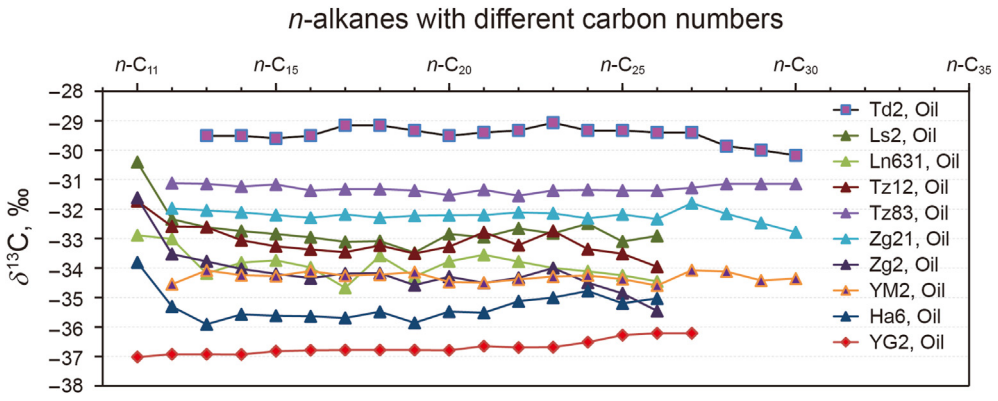

Fig. 9. Compound-specific $\delta^{13}C$ of n-alkanes of typical oil samples.

opposite distribution of C_{28} TAS, METAS, and TDS (Fig. 3a–d), indicating that this oil contained contributions from early-generated oil. Therefore, the oil from Well Tz30 might be a mixture of early-generated and late-generated oils. In addition, under the influence of isotope fractionation during thermal evolution, the carbon isotope difference of crude oil from the same source is generally no more than 3‰ (Peters et al., 2005), whereas the $\delta^{13}C$ difference in compound-specific n-alkanes between oil and oil inclusions from Well Tz421 (3221 m) is more than 5‰ (Fig. 4). This also confirmed the mixing of early-generated and late-generated oils.

4.3. Mixing of oils from different sources

Crude oils from different sources have different biomarkers and isotopes (Peters et al., 2005). Almost all Lower-Paleozoic marine crude oils in the Tarim Basin are derived from two types of source rocks, one of which is rich in TDS and Ai and deficient in C_{28} TAS and METAS, whereas the other shows the opposite characteristics (Sun et al., 2003; Huang et al., 2016; He et al., 2020a, 2022b). Most of the crude oils in the Tazhong and Tabei areas have abundant aryl isoprenoids, C_{28} TAS, and METAS levels, but lower TDS levels (typical aryl isoprenoids and TAS are presented in Fig. 3g, h), indicating that

Table 2
Geochemical characteristics of typical marine oil samples in the Tarim Basin.

SN.	$\delta^{13}C$ of whole oil and group components					Relative content of group components			
	Oil, ‰	SA*, ‰	AH, ‰	NH, ‰	AS, ‰	SA, %	AH, %	NH, %	AS, %
WO01	−31.69	−33.94	−31.02	−30.89	/	88.99	9.19	1.82	/
WO02	−29.02	−32.56	−29.30	−29.69	/	93.71	4.86	1.42	/
WO03	−32.55	−35.44	−32.39	−31.59	−31.86	63.60	17.87	15.98	2.55
WO04	−29.55	−34.76	−31.05	−30.13	−28.64	82.31	12.70	4.08	0.91
WO05	−33.03	−35.93	−32.94	−32.75	−33.29	56.85	22.07	15.20	5.88
WO06	−32.06	−34.62	−32.14	−31.83	−32.70	65.56	20.92	11.81	1.71
WO07	−30.16	−29.98	−28.95	−30.00	/	91.40	6.53	2.07	/
WO08	−32.44	−35.64	−32.23	−32.06	−32.53	66.57	17.71	11.94	3.78
WO09	−32.53	−34.58	−32.57	−33.15	−32.23	87.30	8.63	3.89	0.19
WO10	−32.73	−36.11	−32.04	−30.94	−30.84	79.54	15.85	4.19	0.41
WO11	−32.39	−35.54	−31.71	−31.14	−31.91	75.30	16.33	6.63	1.74
WO12	−32.47	−35.28	−31.84	−31.11	−31.02	80.80	13.88	4.86	0.46
WO13	−31.11	−34.29	−29.87	−29.90	/	94.00	5.78	0.22	/
WO14	−32.16	−35.83	−31.24	−30.76	/	88.51	9.08	1.72	0.70
WO15	−30.19	−30.84	−28.72	−30.76	/	91.87	6.29	1.84	/
WO16	−29.87	−32.71	−29.46	−29.60	/	90.25	8.26	1.49	/
WO17	−31.17	−34.07	−29.72	−29.72	/	92.64	6.06	1.03	0.27
WO18	−29.62	−29.98	−29.01	−30.04	/	92.42	6.32	0.88	0.38
WO19	−31.24	−33.31	−29.52	−29.88	/	93.55	5.24	1.20	/
WO20	−31.95	−33.97	−31.43	−31.74	−31.88	61.50	17.85	11.89	8.76
WO21	−28.78	−30.29	−28.21	−28.43	−28.48	64.62	17.26	15.45	2.66
WO22	−31.78	−33.19	−32.08	−31.67	−32.78	39.18	27.02	13.20	20.60
WO23	−30.75	−32.89	−30.01	−29.66	/	86.27	10.40	2.70	0.63
WO24	−29.31	−32.04	−29.03	−29.32	/	92.54	4.93	2.29	0.23
WO25	−31.67	−34.10	−31.04	−30.46	/	92.49	6.27	0.99	0.25
WO26	−28.61	−31.38	−29.31	−29.93	/	94.88	4.35	0.57	0.19
WO27	−31.72	−34.28	−31.34	−30.70	/	89.75	8.30	1.49	0.46
WO28	−33.31	−35.90	−32.76	−32.85	−33.51	49.09	20.22	14.48	16.20
WO29	−34.45	−36.85	−33.14	−32.84	−31.12	81.74	13.33	3.55	1.38
WO30	−32.10	−34.67	−31.83	−31.95	−32.22	65.25	21.11	11.71	1.92
WO31	−31.96	−34.74	−31.13	−31.01	/	91.14	7.27	1.59	/
WO32	−32.89	−35.76	−31.19	−29.69	/	94.13	4.66	1.21	/
WO33	−32.52	−35.34	−31.63	−31.06	−30.93	86.46	11.08	2.37	0.10
WO34	−31.63	−34.45	−31.48	−31.03	/	91.33	7.49	1.18	/
WO35	−31.15	−33.31	−30.96	−30.94	−30.73	71.64	15.55	9.33	3.48

Note: SN., the oil sample number; SA, saturated hydrocarbon; AH, aromatic hydrocarbon; NH, non-hydrocarbon; AS, asphaltene;/, no detected; SA*, $\delta^{13}C$ average value of the medium molecular n-alkanes (nC_{13}-nC_{22}) in the SA.

Table 3
Relative contribution from heavier $\delta^{13}C$ end-member in the mixed oil.

SN.	Contribution from heavy $\delta^{13}C$ end-member, %					
	Oil	SA	AH	NH	AS	Group component
WO01	35.75	100.00	100.00	100.00	100.00	100.00
WO02	94.72	100.00	100.00	100.00	100.00	100.00
WO03	16.83	34.41	22.49	44.88	59.42	34.59
WO04	83.07	51.02	62.59	86.95	100.00	54.40
WO05	6.10	22.45	6.00	11.47	7.95	16.30
WO06	27.68	54.44	29.99	37.99	29.26	46.95
WO07	69.44	100.00	100.00	100.00	100.00	100.00
WO08	19.14	29.55	27.13	31.33	35.20	29.54
WO09	17.13	55.31	17.01	0.00	46.01	49.84
WO10	12.75	17.96	32.87	63.63	96.03	22.56
WO11	20.22	32.04	42.71	58.01	57.63	35.95
WO12	18.65	38.24	39.07	58.75	89.57	39.59
WO13	48.48	62.38	97.80	93.79	nd	64.49
WO14	25.49	24.93	56.75	68.89	nd	29.10
WO15	68.77	100.00	100.00	100.00	100.00	100.00
WO16	75.97	100.00	100.00	100.00	100.00	100.00
WO17	47.32	67.71	99.48	98.76	nd	70.04
WO18	81.46	100.00	100.00	100.00	100.00	100.00
WO19	45.79	100.00	100.00	100.00	100.00	100.00
WO20	29.98	70.26	51.26	40.76	58.71	62.35
WO21	100.00	100.00	100.00	100.00	100.00	100.00
WO22	33.81	89.24	31.68	42.68	26.28	54.57
WO23	56.60	96.66	93.86	100.00	nd	96.48
WO24	88.20	100.00	100.00	100.00	100.00	100.00
WO25	36.20	67.08	62.86	77.39	nd	67.00
WO26	87.64	100.00	100.00	100.00	100.00	100.00
WO27	35.12	62.71	53.88	70.53	nd	62.26
WO28	0.00	23.06	11.29	8.69	0.00	14.86
WO29	0.00	0.00	0.00	9.01	86.13	1.51
WO30	26.80	53.25	39.18	34.71	46.24	47.98
WO31	29.81	51.44	60.12	61.67	nd	52.24
WO32	9.24	26.53	58.37	99.65	nd	28.90
WO33	17.47	36.80	45.16	60.36	92.93	38.34
WO34	37.03	58.55	49.69	61.07	nd	57.91
WO35	47.63	100.00	100.00	100.00	100.00	100.00

Note: SA, saturated hydrocarbon; AH, aromatic hydrocarbon; NH, non-hydrocarbon; AS, asphaltene; nd, no data.

two types of source rocks at the same time contributed to these oils (Li et al., 2015; Huang et al., 2016; Pang et al., 2016).

5. Quantitative analytical model of mixed oil and its application

5.1. Establishment of conceptual model

Petroleum discovered in the Tarim Basin varies dramatically from condensate to light oil, normal oil, waxy oil, heavy oil, and solid bitumen, as well as from light in color to yellow to black (Huang et al., 2016). The oil group compositions in the study area are also remarkably different, with the highest contents of SAs, AH, NH, and AS, being 94.88%, 21.11%, 15.98%, and 3.78%, respectively, and the lowest contents being as high as 39.18%, 4.35%, 0.22% and 0%, respectively. The average values were 81%, 12%, 5%, and 2%, respectively (Fig. 5a and b). These differences indicated that the oil in the study area is a mixture of four group components with different relevant contents, just like the simulation experiment in which these oils were found to be the result of light oil (replaced by dichloromethane, representing the oil dominated by SAs and AH) diluting heavy oil (WO30, representing the oil dominated by NH and AS) in different proportions (Fig. 5c). Considering the small change in $\delta^{13}C$ in oil during the liquid hydrocarbon generation of kerogen (Fig. 6), the mixed oil in the current reservoir must be understood as a remixed hydrocarbon of a mixture of SAs, AH, NH, and AS in different proportions, as presented in the conceptual model (Fig. 7).

Table 4
$\delta^{13}C$ composition of end-member oil from the Tarim Basin.

Type	$\delta^{13}C_{SA}$, ‰	$\delta^{13}C_{AH}$, ‰	$\delta^{13}C_{NH}$, ‰	$\delta^{13}C_{AS}$, ‰	$\delta^{13}C_{Oil}$, ‰
LCIE	−36.85	−33.14	−33.15	−33.51	−33.31
HCIE	−32.75	−29.80	−29.68	−30.73	−28.78

Note: LCIE, lighter $\delta^{13}C$ end-member; HCIE, heavier $\delta^{13}C$ end-member; SA, saturated hydrocarbon; AH, aromatic hydrocarbon; NH, non-hydrocarbon; AS, asphaltene.

5.2. Quantitative analytical method

The thermal simulation of oil (from Well S47 in the Tabei Uplift) in the Tarim Basin simulates the process of thermal alteration of underground liquid hydrocarbons in the reservoir (Liu, 2008). The $\delta^{13}C$ values of the original oil, free oil (flowable oil in the reservoir), residue oil (mineral-bound hydrocarbon or unflowable oil in the reservoir), and their group component (SAs, AH, NH, and AS) were tested. We found that the $\delta^{13}C$ of residue oils and their four group components gradually became heavier with increasing thermal alteration temperature, while the $\delta^{13}C$ of free oils and their four group components did not significantly change with an increase in thermal alteration temperature (Fig. 8). This finding indicated that the $\delta^{13}C$ of the flowable liquid hydrocarbon and its four group components in the reservoir was highly stable during the process of thermal alteration. Additionally, large amounts of research have been conducted on the impact of secondary alterations on oil. Slight biodegradation mainly destroys small-molecular SAs. When the degradation becomes more severe, all SAs are completely destroyed (Peters et al., 2005). Gas washing mainly causes the loss of small molecular SAs (especially n-alkanes) but has little effect on macromolecular SAs (Zhu et al., 2014; Zhang et al., 2010). Thermochemical sulfate reduction (TSR) might preferentially destroy small molecular hydrocarbons, resulting in heavier $\delta^{13}C$ in the remaining low-carbon-number SAs (Cai et al., 2015). Especially for oil with abundant thioadamantane (indicating severe TSR) from Well Zs1C, the compound-specific $\delta^{13}C$ of n-alkane decreased from −26.73‰ (nC_{11}) to −33.02‰ (nC_{25}) with an increase in the carbon number in this study. Additionally, as the compound-specific $\delta^{13}C$ of medium molecular n-alkanes (MMA) had similar values in this (Fig. 9) and previous studies (Cai et al., 2015; Li et al., 2015; Pang et al., 2016), we think that the compound-specific $\delta^{13}C$ of MMA maintains high stability and may indicate the $\delta^{13}C$ information of the SAs before the second alteration, meaning that the $\delta^{13}C$ average of MMA can be used to calculate the mixing ratio of SAs in mixed oil. Thus, the second alteration had little or no effect on the $\delta^{13}C$ of MMA, AH, NH and AS in the free oil. According to the material balance model (Pang et al., 2016), the $\delta^{13}C$ values of MMA, AH, NH, and AS from mixed oil can be used to calculate the hydrocarbon mixing ratio under the appropriate choice of $\delta^{13}C$ end-member.

According to present and previous studies (Huang et al., 2016; Chen et al., 2018; He et al., 2020a), as well as the relevant studies on the correlation of oil with stable and reliable aromatic biomarker indices (including TAS, TDS, 3-methyl-24-ethyl-triaromatic sterane, and aryl isoprenoids) in this study, we think that all the oil from the SWTBA is from the same type of source rock (the Lower Cambrian and Middle-Lower Ordovician) based on cluster analysis and discriminant analysis (Suppl. Figs. S1–S5, details will be discussed in another paper). These crude oils have heavier $\delta^{13}C$ values. Since absolute EMO might not exist in the Tarim Basin (Huang et al., 2016), we took the $\delta^{13}C$ average of the group component from oil with a clear source in the SWTBA as the appropriate heavier $\delta^{13}C$ end-member. We took the lightest $\delta^{13}C$ average of the group component from oil in the Tazhong and Tabei Uplifts as the

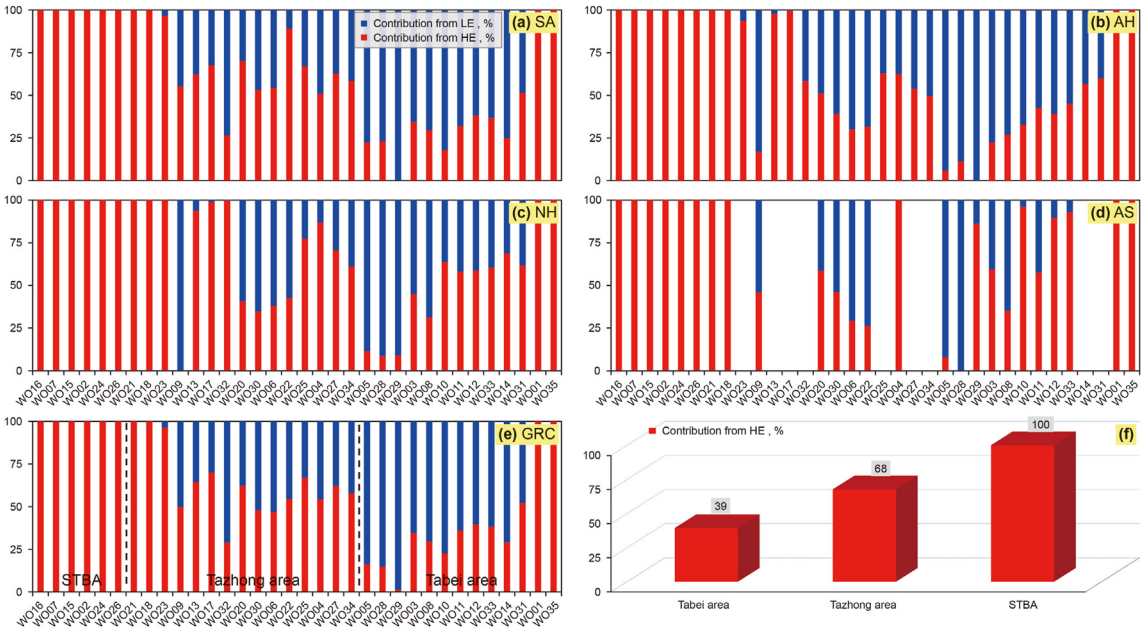

Fig. 10. Quantitative analysis results of mixed oil (Note: SA, saturated hydrocarbon; AH, aromatic hydrocarbon; NH, non-hydrocarbon; AS, asphaltene; GRC, group components; STBA, southwest Tarim Basin area; LE, end-member oil with lighter $\delta^{13}C$; HE, end-member oil with heavier $\delta^{13}C$).

appropriate lighter $\delta^{13}C$ end-member to eliminate the influence of secondary alterations (which mainly cause $\delta^{13}C$ heavier).

Therefore, on the basis of the above analysis and the principle of material balance, we obtained the comprehensive mixing proportion of EMO by calculating the weighted average of mixing proportions from SAs, AH, NH and AS on their relative concentrations.

$$\delta^{13}C_{Emai} = ave\left\{\delta^{13}C_{ai}\right\} \quad \text{Eq-1}$$

$$\delta^{13}C_{Embi} = ave\left\{\delta^{13}C_{bi}\right\} \quad \text{Eq-2}$$

$$\delta^{13}C_{oili} = \delta^{13}C_{Emai} \times f_i + \delta^{13}C_{Embi} \times (1 - f_i) \quad \text{Eq-3}$$

$$F = \sum \frac{C_i \times f_i}{100} \quad \text{Eq-4}$$

where Em is the end-member oil; a and b indicate the EMO with heavier and lighter $\delta^{13}C$, respectively; i indicates SAs (MMA), AH, NH, and AS; f_i is the relative contribution of component i of Ema to that of mixed oil (%); ave $\{\delta^{13}C_{ai}\}$ is the average $\delta^{13}C$ value of component i from Ema (‰); min $\{\delta^{13}C_{bi}\}$ is the minimum $\delta^{13}C$ value of component i from Emb (‰); $\delta^{13}C_{oili}$, $\delta^{13}C_{Emai}$, and $\delta^{13}C_{Embi}$ are the $\delta^{13}C$ of component i from mixed oil, Ema, and Emb, respectively, in which the $\delta^{13}C$ average of the SAs is replaced by that of MMA; F is the comprehensive contribution of Ema to the whole mixed oil (%); and C_i is the relative mass percentage of component i in the oil (%).

For mixed oil, F should be between 0 and 100, indicating the relative contribution of the EMO with heavier $\delta^{13}C$ to mixed oil. If $F > 100$, the oil is mainly composed of EMO with heavier $\delta^{13}C$ and has undergone serious secondary alteration. If $F < 0$, the constructed theoretical group component end-member with lighter $\delta^{13}C$ is unreasonable (the minimum value is not considered), and the theoretical end-member needs to be reconstructed to recalculate the mixing ratio.

According to the testing results (Table 2) and data reported in previous studies (Huang et al., 2016; Pang et al., 2016; Chen et al., 2018), the mixing ratios (Table 3) were calculated based on the $\delta^{13}C$ end-members of oils and their four group components (Table 4).

5.3. Application to the Tarim Basin and its geological significance

Theoretically, the mixing ratio calculation results of different components should be consistent or similar; however, the mixing ratios calculated based on different end-members considerably varied (Figs. 10–11), which may have been due to the large difference in the relative contents of the components. Typically, for the WO31 oil from Well Rp3 (6977.2–7040 m, light oil) with 91.14% SAs, 7.27% AH, 1.59% NH, and 0% AS, the calculated mixing ratios based on the whole oil, SAs, AH, NH, AS, and four group components were 29.81%, 51.44%, 60.12%, 61.67%, 0%, and 52.24%, respectively. For the WO22 oil from Well Tz12 (4339.5–4413.5 m, heavy oil) with 39.18% SAs, 27.02% AH, 13.20% NH and 20.60% AS, the calculated mixing ratios based on the whole oil, SAs, AH, NH, AS, and four group components were 33.81%, 89.24%, 31.68%, 42.68%, 26.28%, and 54.57%, respectively. Moreover, probably due to the influence of secondary alterations, comparisons based on the mixing ratio between GRC and SAs (mainly MMA), AH, NH, and AS showed that (1) the mixed ratios of GRC and SAs are consistent for light oil, but not for heavy oil, such as the WO22 oil sample (the latter overestimated the contribution of EMO with heavier $\delta^{13}C$) (Fig. 11a); (2) the mixed ratios of GRC, AH, NH, and AS are inconsistent for both light and heavy oils, and the latter three overestimate or underestimate the contribution of EMO with heavier $\delta^{13}C$ to varying degrees (Fig. 11b–d); and (3) the mixed ratios for GRC and the whole oil are also inconsistent, where the latter overestimates the contribution of end-member oil with heavier $\delta^{13}C$ for heavy oils while underestimating that for light oils. The differences discussed above indicate that (1) the traditional $\delta^{13}C$ method for whole oil cannot be used to effectively de-convolute deep mixed oil because of the

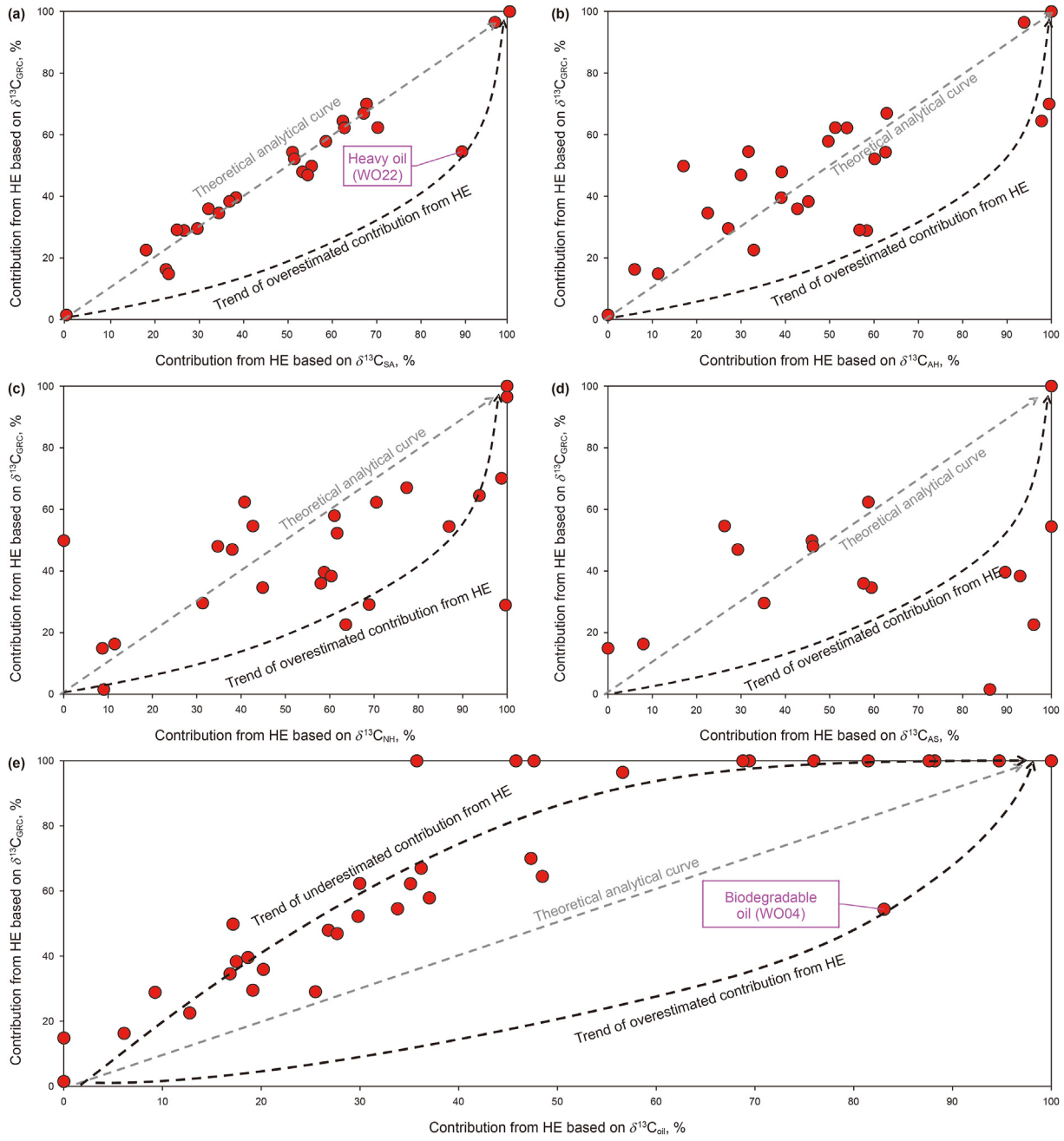

Fig. 11. Comparison of quantitative analysis results of mixed oil obtained by different methods (Note: SA, saturated hydrocarbon; AH, aromatic hydrocarbon; NH, non-hydrocarbon; AS, asphaltene; GRC, group components; HE, end-member oil with heavier $\delta^{13}C$).

absence of absolute end-member oils in the study area; (2) the traditional $\delta^{13}C$ method of compound-specific n-alkanes can effectively de-convolute mixed light oil, but it cannot de-convolute the mixed heavy oil; and (3) the proposed $\delta^{13}C$ method of GRC can not only de-convolute mixed light oil but also mixed heavy oil. Therefore, compared to the traditional $\delta^{13}C$ method of de-convoluting mixed oil, the proposed $\delta^{13}C$ method of group components has a wider range of applications.

In different structural zones, end-member oil with heavier $\delta^{13}C$ strongly contributes to mixed oil in the Tazhong area, with an average contribution proportion of 68%; however, it contributes little to the mixed oil in the Tabei area, with an average contribution of 39%. In this study, oil end-members with heavier $\delta^{13}C$ derived from the Cambrian-Lower Ordovician (specifically the Lower Cambrian Yuertus Formation and Middle-Lower Ordovician Heituao Formation source rocks in this study (ϵ_1y and $O_{1\text{-}2}$h, respectively, Suppl. Figs. S1–S5), whereas oil end-members with lighter $\delta^{13}C$ is derived from the Middle-Upper Ordovician (specifically Middle-Upper Ordovician Lianglitage Formation, Suppl. Figs. S1–S5). Therefore, based on the detailed description of the distribution of effective source rocks, this method will help realize differential exploration, further improve the efficiency of deep liquid hydrocarbon exploration in the Tarim Basin, and have wide application potential for deep complex mixed oil in international basins.

6. Conclusions

(1) Mixed oil is common in the Tarim Basin, mainly including a mix of biodegraded and non-biodegraded oil, early- and late-generated oil, and oils from different sources, as evidenced by stable aromatic biomarkers and compound-specific $\delta^{13}C$ of n-alkanes in oil and/or oil inclusions. Mixed oil varies dramatically in color and density, which exceeds the capabilities of traditional biomarker and isotope technology to de-convolute mixed oil.
(2) The proposed $\delta^{13}C$ method of group components to de-convolute mixed oil revealed the relative contribution of end-member oils, which can help in the differential exploration of deep complex mixed oil in different structural zones.
(3) Compared to the traditional $\delta^{13}C$ method using whole oil or compound-specific n-alkanes to de-convolute mixed oil, the proposed $\delta^{13}C$ method of group components has a wider range of applications, including various complex mixed oils from light to heavy oil. This might promote the exploration of deep complex mixed oil around the world.

Availability of data and material

Detailed information describing the experimental data is in the main text.

Author contributions

Tao-Hua He, conceptualization and writing the original draft; Wen-Hao Li and Shuang-Fang Lu, Supervision and Conceptualization; Er-Qiang Yang and Tao-Tao Jing, Software and Methodology; Jun-Feng Ying and Peng-Fei Zhu, Investigation; Xiu-Zhe Wang and Zhong-Hong Chen, Writing - Review & Editing; Wen-Qing Pan and Bao-Shou Zhang, Resources. All authors commented on the previous version and approved the final version of this manuscript.

Declaration competing interest

We confirm that there are no known conflicts of interest associated with this publication and there has been no significant financial support for this work that could have influenced its outcome. We confirm that the manuscript has been read and approved by all named authors and that there are no other persons who satisfied the criteria for authorship but are not listed. We further confirm that the order of authors listed in the manuscript has been approved by all of us. We confirm that we have given due consideration to the protection of intellectual property associated with this work and that there are no impediments to publication, including the timing of publication, with respect to intellectual property. In so doing we confirm that we have followed the regulations of our institutions concerning intellectual property.

Acknowledgments

The authors are grateful for the financial supports provided by the National Science and Technology Major Project of the Ministry of Science and Technology of China (2016ZX04004-004), National Natural Science Foundation of China (41672125). We appreciate Petroleum Exploration & Production Research Institute, Tarim Oilfield Company for providing some geochemical data of oil inclusions and arranging access to the oil and source rocks. Besides, special thanks are given to the journal editor and four anonymous reviewers for their helpful comments and suggestions which improved the manuscript.

Appendix A. Supplementary data

Supplementary data to this article can be found online at https://doi.org/10.1016/j.petsci.2022.07.010.

References

Arouri, K.R., McKirdy, D.M., 2005. The behaviour of aromatic hydrocarbons in artificial mixtures of Permian and Jurassic end-member oils: application to in-reservoir mixing in the Eromanga Basin, Australia. Org. Geochem. 36, 105–115. https://doi.org/10.1016/j.orggeochem.2004.06.015, 2005.
Cai, C.F., Li, K.K., Ma, A.L., et al., 2009. Distinguishing Cambrian from Upper Ordovician source rocks: evidence from sulfur isotopes and biomarkers in the Tarim Basin. Org. Geochem. 40, 755–768. https://doi.org/10.1016/j.orggeochem.2009.04.008.
Cai, C.F., Zhang, C.M., Worden, R.H., et al., 2015. Application of sulfur and carbon isotopes to oil–source rock correlation: a case study from the Tazhong area. Tarim Basin, China. Org. Geochem. 83, 140–152. https://doi.org/10.1016/j.orggeochem.2015.03.012.
Chen, C.S., Wang, Y.P., Beagle, J.R., et al., 2019. Reconstruction of the evolution of deep fluids in light oil reservoirs in the Central Tarim Basin by using PVT simulation and basin modeling. Mar. Petrol. Geol. 107, 116–126. https://doi.org/10.1016/j.marpetgeo.2019.05.009.
Chen, J.P., Deng, C.P., Liang, D.G., et al., 2003. Mixed oils derived from multiple source rocks in the Cainan oilfield, Junggar Basin, Northwest China. Part II: artificial mixing experiments on typical crude oils and quantitative oil-source correlation. Org. Geochem. 34, 911–930. https://doi.org/10.1016/S0146-6380(03)00031-7.
Chen, J.P., Deng, C.P., Song, F.Q., et al., 2007. A mathematical calculation model using biomarkers to quantitatively determine the relative source proportion of mixed oil. Acta Geol. Sin. 81, 817–826. https://doi.org/10.1111/j.1755-6724.2007.tb01005.x.
Chen, Z.H., Wang, T.G., Li, M.J., et al., 2018. Biomarker geochemistry of crude oils and Lower Paleozoic source rocks in the Tarim Basin, western China: an oil-source rock correlation study. Mar. Petrol. Geol. 96, 94–112. https://doi.org/10.1016/j.marpetgeo.2018.05.023.
Cheng, B., Liu, H., Cao, Z.C., et al., 2020. Origin of deep oil accumulations in carbonate reservoirs within the north Tarim Basin: insights from molecular and isotopic compositions. Org. Geochem. 139, 103931. https://doi.org/10.1016/j.orggeochem.2019.103931.
Dzou, L.I., Holba, A.G., Ramón, J.C., et al., 1999. Application of new diterpane biomarkers to source, biodegradation and mixing effects on Central Llanos Basin oils, Colombia. Org. Geochem. 30, 515–534. https://doi.org/10.1016/S0146-6380(99)00039-X.
He, T.H., Lu, S.F., Li, W.H., et al., 2018. Effect of salinity on source rock formation and its control on the oil content in shales in the Hetaoyuan Formation from the Biyang Depression, Nanxiang Basin, Central China. Energy Fuels 32, 6698–6707. https://doi.org/10.1021/acs.energyfuels.8b01075.
He, T.H., Li, W.H., Lu, S.F., et al., 2022b. Distribution and isotopic signature of 2-alkyl-1,3,4-trimethylbenzenes in the Lower Paleozoic source rocks and oils of Tarim Basin: implications for the oil-source correlation. Petrol. Sci. (in press).
He, T.H., Li, W.H., Tan, Z.Z., et al., 2019. Mechanism of shale oil accumulation in the hetaoyuan formation from the biyang depression, nanxiang basin. Oil Gas Geol. 40 (6), 1259–1269 (in Chinese).
He, T.H., Lu, S.F., Li, W.H., et al., 2020a. Geochemical characteristics and effectiveness of thick, black shales in southwestern depression. Tarim Basin. J. Petrol. Sci. Eng. 185, 106607. https://doi.org/10.1016/j.petrol.2019.106607.
He, T.H., Lu, S.F., Li, W.H., et al., 2020b. Paleoweathering, hydrothermal activity and organic matter enrichment during the formation of earliest Cambrian black strata in the northwest Tarim Basin, China. J. Petrol. Sci. Eng. 189, 106987. https://doi.org/10.1016/j.petrol.2020.106987.
He, T.H., Li, W.H., Lu, S.F., et al., 2022a. Mechanism and geological significance of anomalous negative $\delta^{13}C_{kerogen}$ in the lower cambrian, NW Tarim Basin, China. J. Petrol. Sci. Eng. 208, 109384. https://doi.org/10.1016/j.petrol.2021.109384.
Hu, T., Pang, X.Q., Jiang, F.J., et al., 2021a. Movable oil content evaluation of lacustrine organic-rich shales: methods and a novel quantitative evaluation model. Earth Sci. Rev. 214, 103545. https://doi.org/10.1016/j.earscirev.2021.103545.
Hu, T., Pang, X.Q., Jiang, F.J., et al., 2021b. Key factors controlling shale oil enrichment in saline lacustrine rift basin: implications from two shale oil wells in Dongpu Depression, Bohai Bay Basin. Petrol. Sci. 18, 687–711. https://doi.org/10.1007/s12182-021-00564-z.
Huang, H.P., Zhang, S.C., Su, J., 2016. Palaeozoic oil–source correlation in the Tarim

Basin, NW China: a review. Org. Geochem. 94, 32–46. https://doi.org/10.1016/j.orggeochem.2016.01.008.
Huang, H.P., Zhang, S.C., Gu, Y., et al., 2017. Impacts of source input and secondary alteration on the extended tricyclic terpane ratio: a case study from Palaeozoic sourced oils and condensates in the Tarim Basin, NW China. Org. Geochem. 112, 158–169. https://doi.org/10.1016/j.orggeochem.2017.07.012.
Li, J.Q., Lu, S.F., Zhang, P.F., et al., 2020. Estimation of gas-in-place content in coal and shale reservoirs: a process analysis method and its preliminary application. Fuel 259, 116266. https://doi.org/10.1016/j.fuel.2019.116266.
Li, M.J., Wang, T.G., Lillis, P.G., et al., 2012. The significance of 24-norcholestanes, triaromatic steroids and dinosteroids in oils and Cambrian–Ordovician source rocks from the cratonic region of the Tarim Basin, NW China. Appl. Geochem. 27, 1643–1654. https://doi.org/10.1016/j.apgeochem.2012.03.006.
Li, S.M., Amrani, A., Pang, X.Q., et al., 2015. Origin and quantitative source assessment of deep oils in the Tazhong Uplift. Tarim Basin. Org. Geochem. 78, 1–22. https://doi.org/10.1016/j.orggeochem.2014.10.004.
Li, W.B., Li, J.Q., Lu, S.F., et al., 2022. Evaluation of gas-in-place content and gas-adsorbed ratio using carbon isotope fractionation model: A case study from Longmaxi shales in Sichuan Basin, China. Int. J. Coal Geol. 249, 103881. https://doi.org/10.1016/j.coal.2021.103881.
Li, W.H., Lu, S.F., Tan, Z.Z., et al., 2017. Lacustrine source rock deposition in response to co-evolution of paleoenvironment and formation mechanism of organic-rich shales in the Biyang Depression, Nanxiang Basin. Energy Fuels 31, 13519–13527. https://doi.org/10.1021/acs.energyfuels.7b02880.
Liu, G.X., 2008. Thermal simulation study of crude oil from well S74 in the Tarim Basin. Part I: geochemical characteristics of the simulation products. Petroleum Geology and Experiment 30 (2), 179–185 (in Chinese).
Pan, W.Q., Chen, Y.Q., Xiong, Y.X., et al., 2015. Sedimentary facies research and implications to advantaged exploration regions on lower cambrian source rocks, Tarim Basin. Nat. Gas Geosci. 26 (7), 1224–1232 (in Chinese).
Pang, X.Q., Chen, J.Q., Li, S.M., et al., 2016. Evaluation method and application of the relative contribution of marine hydrocarbon source rocks in the Tarim Basin: a case study from the Tazhong area. Mar. Petrol. Geol. 77, 1–18. https://doi.org/10.1016/j.marpetgeo.2016.05.023.
Peters, K.E., Walters, C.C., Moldowan, J.M., 2005. The Biomarker Guide: Biomarkers and Isotopes in Petroleum Exploration and Earth History. Cambridge University Press, Cambridge, pp. 1–471.
Peters, K.E., Ramos, L.S., Zumberge, J.E., et al., 2008. Deconvoluting mixed crude oil in prudhoe bay field, north slope, Alaska. Org. Geochem. 39, 623–645. https://doi.org/10.1016/j.orggeochem.2008.03.001.
Sun, D.Q., Liu, X.P., Li, W.H., et al., 2022. Quantitative evaluation the physical properties evolution of sandstone reservoirs constrained by burial and thermal evolution reconstruction: A case study from the Lower Cretaceous Baxigai Formation of the western Yingmaili Area in the Tabei Uplift, Tarim Basin, NW China. J. Petrol. Sci. Eng. 208, 109460. https://doi.org/10.1016/j.petrol.2021.109460.
Sun, Y.G., Xu, S.P., Lu, H., et al., 2003. Source facies of the Paleozoic petroleum systems in the Tabei uplift, Tarim Basin, NW China: implications from aryl isoprenoids in crude oils. Org. Geochem. 34, 629–634. https://doi.org/10.1016/S0146-6380(03)00063-9.
Tian, H., Xiao, X.M., Wilkins, R.W.T., et al., 2008. Formation and evolution of silurian paleo-oil pools in the Tarim Basin, NW China. Org. Geochem. 39, 1281–1293. https://doi.org/10.1016/j.orggeochem.2008.05.011.
Xiao, Z.Y., Li, M.J., Huang, S.Y., et al., 2016. Source, oil charging history and filling pathways of the Ordovician carbonate reservoir in the Halahatang Oilfield, Tarim Basin, NW China. Mar. Petrol. Geol. 73, 59–71. https://doi.org/10.1016/j.marpetgeo.2016.02.026.
Yang, H.J., Chen, Y.Q., Tian, J., et al., 2020. Great discovery and its signifi cance of ultra-deep oil and gas exploration in well Luntan-1 of the Tarim Basin. China Petroleum Exploration 25 (2), 62–72. https://doi.org/10.3969/j.issn.1672-7703.2020.02.007 (in Chinese).
Yu, S., Pan, C.C., Wang, J.J., et al., 2012. Correlation of crude oils and oil components from reservoirs and source rocks using carbon isotopic compositions of individual n-alkanes in the Tazhong and Tabei Uplift of the Tarim Basin. China. Org. Geochem. 52 (1), 67–80. https://doi.org/10.1016/j.orggeochem.2012.09.002.
Zhan, Z.W., Zou, Y.R., Shi, J.T., et al., 2016. Unmixing of mixed oil using chemometrics. Org. Geochem. 92, 1–15. https://doi.org/10.1016/j.orggeochem.2015.11.006.
Zhang, B., Huang, L., Ying, W., et al., 2010. Quantitative evaluation of crude oil composition changes caused by strong gas washing: a case study of natural gas pool in Kuqa Depression. Earth Sci. Front. 17 (4), 270–279 (in Chinese).
Zhang, S.C., Liang, D.G., Zhang, B.M., et al., 2004a. Marine Petroleum Formation in Tarim Basin (In Chinese). Petroleum Industry Press, Beijing, pp. 1–433 (in Chinese).
Zhang, J., Pang, X.Q., Liu, L.F., et al., 2004b. Distribution characteristics and petroleum geological significance of the Silurian asphaltic sandstones in Tarim Basin. Science in China (Series D: Earth Sci. 47, 199–208. https://doi.org/10.1360/04zd0039.
Zhang, S.C., Huang, H.P., Su, J., et al., 2015. Ultra-deep liquid hydrocarbon exploration potential in cratonic region of the Tarim Basin inferred from gas condensate genesis. Fuel 160, 583–595. https://doi.org/10.1016/j.fuel.2015.08.023.
Zhang, Y.Y., Zwingmann, H., Liu, K.Y., et al., 2011. Hydrocarbon charge history of silurian sandstone reservoirs in the Tazhong uplift, Tarim Basin, China. AAPG Bull. 95, 395–412. https://doi.org/10.1306/08241009208.
Zhu, G.Y., Zhang, S.C., Su, J., et al., 2012. The occurrence of ultra-deep heavy oils in the Tabei Uplift of the Tarim Basin, NW China. Org. Geochem. 52, 88–102. https://doi.org/10.1016/j.orggeochem.2012.08.012.
Zhu, G.Y., Zhang, B.T., Yang, H.J., et al., 2014. Secondary alteration to ancient oil reservoirs by late gas filling in the Tazhong area. Tarim Basin. J. Petrol. Sci. Eng. 122, 240–256. https://doi.org/10.1016/j.petrol.2014.07.017.
Zhu, G.Y., Milkov, A.V., Chen, F.R., et al., 2018. Non-cracked oil in ultra-deep high-temperature reservoirs in the Tarim Basin, China. Mar. Petrol. Geol. 89, 252–262. https://doi.org/10.1016/j.marpetgeo.2017.07.019.
Zhu, G.Y., Zhang, Z.Y., Zhou, X.X., et al., 2019a. The complexity, secondary geochemical process, genetic mechanism and distribution prediction of deep marine oil and gas in the Tarim Basin, China. Earth Sci. Rev. 198, 102930. https://doi.org/10.1016/j.earscirev.2019.102930.
Zhu, G.Y., Zhang, Y., Zhou, X.X., et al., 2019b. TSR, deep oil cracking and exploration potential in the Hetianhe gas field, Tarim Basin, China. Fuel 236, 1078–1092. https://doi.org/10.1016/j.fuel.2018.08.119.
Zhu, G.Y., Li, J.F., Zhang, Z.Y., et al., 2020. Stability and cracking threshold depth of crude oil in 8000 m ultra-deep reservoir in the Tarim Basin. Fuel 282, 118777. https://doi.org/10.1016/j.fuel.2020.118777.